

# Detection of delayed gamma-ray emissions around supernova remnant HB9 using Fermi-LAT observations

Tomohiko Oka<sup>a,b,\*</sup> and Wataru Ishizaki<sup>c</sup>

<sup>a</sup>Department of Physical Sciences, Ritsumeikan University, Kusatsu, Shiga 525-8577, Japan

<sup>b</sup>Research Organization of Science and Technology, Ritsumeikan University, Kusatsu, Shiga 525-8577, Japan

<sup>c</sup>Center for Gravitational Physics, Yukawa Institute for Theoretical Physics, Kyoto University, Kyoto, Kyoto 606-8502, Japan

E-mail: [toka2023@gst.ritsumei.ac.jp](mailto:toka2023@gst.ritsumei.ac.jp), [wataru.ishizaki@yukawa.kyoto-u.ac.jp](mailto:wataru.ishizaki@yukawa.kyoto-u.ac.jp)

Cosmic ray (CR) protons that escaped from supernova remnants (SNRs) illuminate surrounding molecular clouds (MCs) and then emit hadronic gamma rays. Since it takes the diffusion time to reach MCs after escaping from SNRs, the gamma-ray spectrum reflects the past distribution of accelerated particles in the SNR. Therefore, such emissions are called “delayed” gamma rays. We analyzed 12-yr Fermi-LAT data around SNR HB9 and detected gamma-ray emissions not only at the SNR shell, as found in previous studies, but also at MCs. The energy spectra at the cloud regions were fitted with a simple power-law function ( $dN/dE \propto E^{-\Gamma}$ ) in an energy range of 1–500 GeV, resulting in a flatter spectral index ( $\Gamma \sim 1.8$ ) than that of the SNR shell ( $\Gamma = 2.55 \pm 0.10$ ). Spectral modeling results show that the spectra of molecular clouds can be reproduced with emissions of protons that escaped in the past from the SNR, the so-called delayed gamma rays. By comparing the energy spectra at the molecular cloud regions and the SNR shell, we investigated a time evolution of the maximum energy of CRs accelerated in the SNR. We then found evidence that this SNR accelerated CRs up to higher energies in the past than the present shell. The obtained lower limit on the maximum energy is  $> 10$  TeV, which will be determined better with TeV gamma-ray observations. We also found that the diffusion coefficient around HB9 is equivalent to the Galactic mean, suggesting that CR-self confinement is inefficient in this region. These results have been presented in the publication [1], to which we refer readers for details.

38th International Cosmic Ray Conference (ICRC2023)  
26 July - 3 August, 2023  
Nagoya, Japan



\*Speaker

## 1. Introduction

Although the origin of cosmic rays (CRs) is still unknown a century after their discovery, supernova remnants in our Galaxy are believed to be the primary origin of CRs up to PeV, mainly in terms of the explosion energy budget [2]. The modern challenge is, however, that few proton accelerations up to PeV energies have been found in observations [e.g., 3]. This discrepancy could be resolved by considering the temporal decay of the maximum particle energy in SNRs [4] as well as the escape from the acceleration site [5]. In other words, it is assumed that the standard SNR can accelerate CRs up to PeV when it is young ( $\sim 100$  yr), but with age, it can no longer accelerate up to such energy, while PeV particles escape from the site at an early stage. To scrutinize this scenario that an SNR has accelerated PeV CRs in the past, it is essential to quantify the evolution of diffusive shock acceleration (DSA) in the SNR.

One reliable way to study the evolution of DSA is the simultaneous gamma-ray observations of the SNR shell part and its nearby molecular clouds (MCs). If a massive cloud exists near the SNR, protons that escape the SNR illuminate the cloud and generate gamma-ray emission via the  $\pi^0$ -decay process [5, 6]. The delay of the timing of the gamma-ray emission from the cloud region from that of the incident proton escape depends on the propagation time and accordingly reflects the particle distribution in the SNR at a specific epoch in the past. Hence, comparing the spectra at the SNR shell and nearby clouds observed at roughly the same time enables us to quantify the evolution of the DSA in the SNR. Such “delayed” gamma rays have been found in the vicinity of some SNRs [7, 8], but none have simultaneously detected gamma-ray emission from shell sections that reflect the current age.

For the application of the measurement, we focus on SNR HB9 (G160.9+2.6), which is relatively young ( $\sim 6.6 \times 10^3$  yr; Leahy & Tian [9]) compared with other objects where delayed gamma-rays have been observed. HB9 has two additional advantages for this type of study in the DSA evolution. Firstly, there are MCs in the vicinity of this SNR, but their locations do not coincide with the SNR in the line of sight [10], enabling us to simply use the distance between the SNR and clouds to calculate the diffusion time. Secondly, HB9 has observable gamma-ray emission from the SNR shell [11], which is essential to estimate the current maximum energy of the accelerated particles at the SNR shock.

While the GeV emission from the shell has been found [11], no detection of the delayed gamma-ray emission have been detected at the nearby MC region. Furthermore, Sezer et al. [10] analyzed the *Fermi*-LAT 10-year data in an energy range between 0.2 and 300 GeV and newly detected a point-like source near the SNR shell, named PS J0506.5+4546. In this work, we examine the gamma-ray morphology of SNR HB9 and the spectra of the SNR shell and the nearby cloud regions, using 12-year observations with the *Fermi*-LAT, with the aim of quantification of the time evolution of DSA.

## 2. Fermi-LAT data analysis

### 2.1 Observations

The *Fermi*-LAT is capable of detecting gamma rays in the GeV band with a wide field of view [12]. We analyze its 12-year data from 2008 August to 2020 August in the vicinity of SNR

HB9. The standard analysis software, Science Tools (version v11r5p3<sup>1</sup>), is used. The ‘Source’ selection criteria and instrument responses (P8R2\_SOURCE\_V6<sup>2</sup>) are chosen, considering a balance between the precision and photon-count statistics. The zenith-angle threshold is set to 90° to suppress the contamination of the background from the Earth rim. We employ the tool `gtlike` (in the binned mode), using a standard maximum likelihood method [13], for spatial and spectral analyses. We choose a square region of 15° × 15° with the center coinciding with that of HB9 (Ra=75.25°, Dec=46.73°) as the region of interest (ROI) for the (binned) maximum likelihood analysis based on Poisson statistics.

The source spatial-distribution model includes all the sources in the fourth Fermi catalog (4FGL; Abdollahi et al. [14]) within the ROI and the two diffuse backgrounds, the Galactic (`gll_iem_v7.fits`) and extragalactic (`iso_P8R3_SOURCE_V2_v1.txt`) diffuse emissions. Regarding the emission of the SNR shell, Araya [11] and Sezer et al. [10] concluded that the radio template produced with the 4850 MHz radio continuum data from the Green Bank Telescope [15] is the best spatial model. Accordingly, we use the radio template provided in the Science Tools as the spatial model. In the fitting of the maximum likelihood analysis, all spectral parameters of HB9 SNR itself, 4FGL sources [14] located within 5° from the center of HB9, and the two diffuse backgrounds are allowed to vary freely. We do not use the data below 1 GeV in this analysis since the fitting results of delayed gamma-ray emission in this band suffer from the systematic uncertainty in the Galactic diffuse background model [16]. The significance of a source is represented in this analysis by the Test Statistic (TS) defined as  $-2\log(L_0/L)$ , where  $L_0$  and  $L$  are the maximum likelihood values for the null hypothesis and a model including additional sources, respectively [13]. The detection significance of the source can be approximated as  $\sqrt{TS}$  when the number of counts is sufficiently large.

## 2.2 Results

The left panel of Fig. 1 shows the background-subtracted gamma-ray TS map created from the *Fermi*-LAT 12-year data above 1 GeV, where the background model consists of the Galactic and isotropic extragalactic emissions and the contributions from the known Fermi sources (see the previous subsection). The map is overlaid with cyan contours of the <sup>12</sup>CO ( $J = 1 - 0$ ) line emission from the Dame survey data [17], which are integrated over a velocity range between  $-10.4$  and  $+2.6$  km s<sup>-1</sup>, and also green contours of 1420 MHz radio continuum emission obtained from the CGPS survey with DRAO [18]. In the right panel of Fig. 1, no significant emission from the SNR shell was found (green contours in the figure), which is consistent with the fact that the SNR spectrum has a cutoff below 10 GeV [11]. The gamma-ray excess appears to be more extended than the point source J0506.5+4546 reported in the previous study [10] and rather spatially coincident with the CO line emission from two distinctive regions (thus two MCs), designated as R1 and R2.

We individually extract Fermi-LAT energy spectra from the radio SNR shell region and the two regions, R1 and R2, and evaluate its detection significance. As for the spatial model for the MC regions, we create a CO template for each of R1 and R2, which is made from the <sup>12</sup>CO ( $J = 1 - 0$ ) line image [17] integrated over a velocity range between  $-10.4$  and  $+2.6$  km s<sup>-1</sup> and cut with a

<sup>1</sup><https://fermi.gsfc.nasa.gov/ssc/data/analysis/software>

<sup>2</sup><https://fermi.gsfc.nasa.gov/ssc/data/Cicerone/>

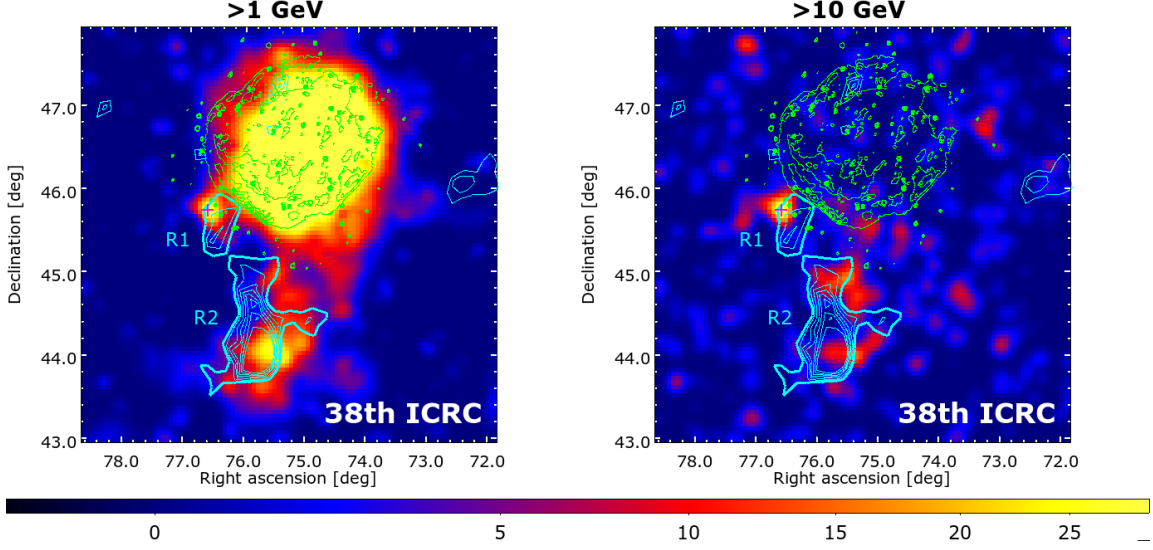


**Figure 1:** Gamma-ray TS maps in the vicinity of SNR HB9 observed with the *Fermi*-LAT. All maps are given with square bins of  $0.05^\circ$ , and Gaussian smoothing with a kernel  $\sigma = 0.1^\circ$  are applied. The energy ranges are (left) 1 to 500 GeV and (right) 10 to 500 GeV. The subtracted background consists of the Galactic and extragalactic diffuse emissions and known gamma-ray source contribution. Green contours show the radio emission of SNR HB9 at 1420 MHz with DRAO [18] and are linearly spaced in increments of 0.5 K from 5.5 K to 10.0 K. Cyan contours show the  $^{12}\text{CO}$  ( $J=1-0$ ) line intensity integrated over a velocity range between  $-10.4$  and  $+2.6$   $\text{km s}^{-1}$  and are linearly spaced in increments of  $1.0$   $\text{K km s}^{-1}$  from 4.5 to 10.5  $\text{K km s}^{-1}$ . The two apparent CO-emission regions (R1 and R2) are indicated. The magenta cross in each panel indicates the position of PS J0506.5+4546 [10].

threshold of  $> 4.5$   $\text{K km s}^{-1}$  (cyan thick-line contours in Figure 1). Figure 2 shows the resultant spectra for an energy range between 1 and 500 GeV. The obtained *Fermi*-LAT spectrum of the SNR shell is consistent with the gamma-ray spectrum reported by [11]. Also, the gamma-ray excesses are detected at the R1 and R2 regions with significances of  $4.5\sigma$  and  $6.1\sigma$ , respectively. Each energy spectrum is fitted with the simple power-law function:  $dN/dE \propto E^{-\Gamma}$ . We then found the spectral indices at the MC regions ( $\Gamma = -1.84 \pm 0.18$  for R1 and  $-1.84 \pm 0.14$  for R2) are flatter than that of the SNR shell ( $\Gamma = -2.55 \pm 0.10$ ). We also found the R1 emission is consistent with PS J0506.5+4546 reported by Sezer et al. [10]. Once we use the point-like source model for R1 instead of the CO template model, the resultant significance is marginally ( $1.3\sigma$  level) improved from the case with the CO template, but the discrepancy of the determined spectral properties (flux and index) between the results of the two spatial-distribution models is smaller than the  $1\sigma$  uncertainty.

### 3. Modeling and Discussion

In this work, we explore the possibility that the R1 and R2 are attributed to the delayed gamma-ray from MCs illuminated by the CRs accelerated in HB9.

The delayed gamma-ray spectra from the MCs are calculated based on the method proposed by Gabici et al. [19] and Ohira et al. [20]. The particle (proton and electron) flux as a function

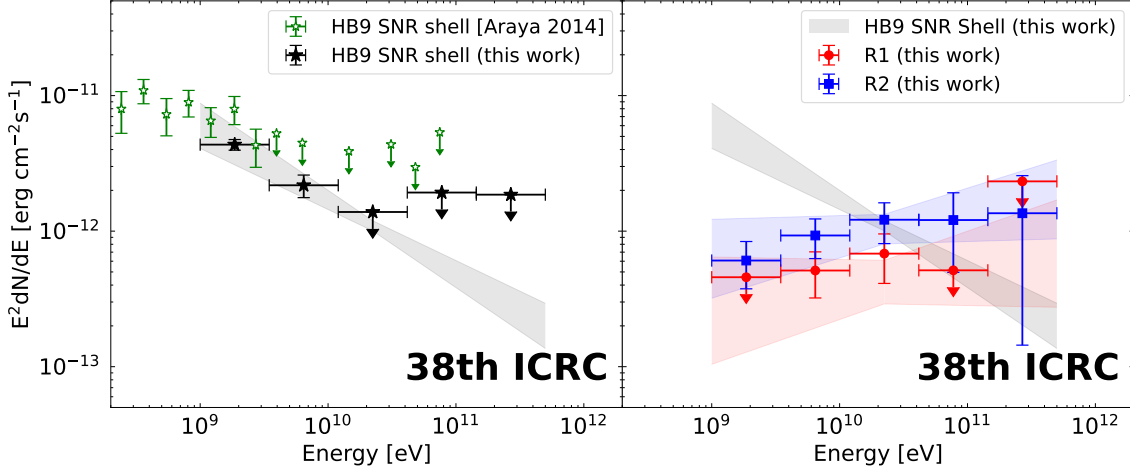


**Figure 2:** Spectral energy distributions measured with the *Fermi*-LAT (data points) and fit results in the gamma-ray band. **Left:** Black and open green stars show the data of the SNR shell obtained in this work and Araya [11], respectively. **Right:** Red and blue data represent the spectra of cloud regions R1 and R2, respectively. Also shown as the shaded black region is the fit result of the SNR shell.

of energy, distance from the SNR, and time is obtained by solving the transport equation. The important assumption is the phenomenological power-law dependence of the cutoff energy  $E_{\text{esc}}$  of the proton spectrum at the SNR shock on the age  $t$  of the SNR, as discussed by [19, 21]:

$$E_{\text{esc}}(t) = E_{\text{max}} \left( \frac{t}{t_{\text{Sedov}}} \right)^{-\alpha}, \quad (1)$$

where  $E_{\text{max}}$  is the maximum energy of the CR protons at  $t_{\text{Sedov}}$  and is set to 3 PeV, and  $\alpha$  is the power-law index that is determined so that the current maximum energy ( $E_{\text{now}}$ ) is equal to  $E_{\text{esc}}(t)$  at the current age  $t_{\text{age}} = 6.6 \times 10^3$  yr [9]. We calculate neutral pion decay for protons, while for electrons, inverse Compton scattering (IC), non-thermal bremsstrahlung, and synchrotron, using the naima package [22]. The details of the model can be found in the recent publication [1].

We attempt to fit the observed spectra of the cloud regions and the SNR shell simultaneously. Fig. 3 shows the modeling results using the model parameters tabulated in Table 2 in [1]. While the multi-wavelength data of the shell can be explained with the leptonic emissions, the MC spectra are mainly explained with the hadronic emissions. The total electron energy and the magnetic field in the SNR shell are in agreement with those estimated by Araya [11], while the electron maximum energy at the shell (corresponding to  $E_{\text{now}}$ ) is determined to be 300 GeV. We found in the simultaneous fitting that the hadronic emission reproduces well the observed spectra even though the assumed parameters in the calculation are typical ones for an SNR and ISM.

We investigate how the model curve varies depending on the input parameters. Here, we show the dependence of the model curve on the diffusion coefficient ( $D_0$ ) and the maximum CR energy in the life ( $E_{\text{max}}$ ) for the R2 spectrum in Fig. 4. The *Fermi*-LAT spectra obtained in this work are found to be well reproduced with the Galactic mean of  $D_0 = 3 \times 10^{28}$  cm<sup>2</sup> s<sup>-1</sup>. Orders of magnitude smaller  $D_0$ , in particular  $D_0 = 3 \times 10^{26}$  cm<sup>2</sup> s<sup>-1</sup>, however, clearly fail to reproduce the observed spectra. In the previous studies for other SNRs [e.g.; 29], the estimated values of  $D_0$

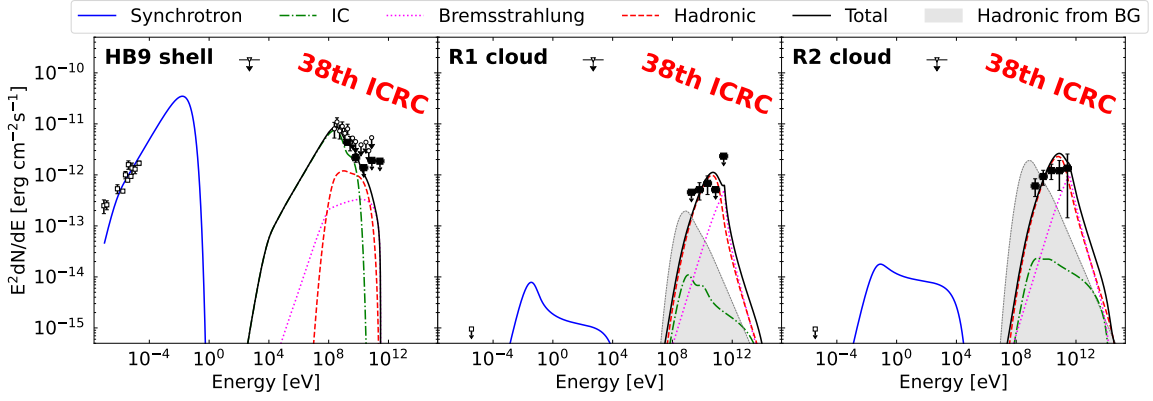


**Figure 3:** Broadband spectral energy distributions of the non-thermal emission from the HB9 shell and the cloud regions. The left, middle, and right panels show the results of the HB9 shell, R1, and R2, respectively. The radio and X-ray data are taken from Leahy & Tian [9], Dwarakanath et al. [23], Reich et al. [24], Roger et al. [25], Gao et al. [26] and Leahy & Aschenbach [27], respectively (see text for detail). The filled squares and open circles show the *Fermi*-LAT data derived in this work and [11], respectively. The lines represent each component of the emission models: synchrotron (blue), electron bremsstrahlung (magenta), IC (green), neutral pion decay (red), and the total gamma-ray emissions (black). In order to demonstrate how much of the Galactic diffuse background at the cloud regions, which may affect the systematic uncertainties in the *Fermi* analysis, we show the hadronic emission from the background CRs with the energy spectrum  $J_{\text{CR}}(E) = 2.2(E/\text{GeV})^{-2.75} \text{ cm}^{-2} \text{ s}^{-1} \text{ GeV}^{-1} \text{ sr}^{-1}$  (e.g., Dermer [28]) as the shaded grey region.

were  $\sim 10$  times smaller than the Galactic mean [30], which were explained in conjunction with self-confinement caused by the generation of turbulent plasma waves [31]. Our diffusion coefficient value, which is close to the Galactic mean, indicates that the excitation of such turbulent plasma waves at the distances to R1 and R2 is inefficient or that the wave damping has a significant effect. We also find that  $E_{\text{max}}$  above 10 TeV still explains the data points. Given that there is a trend for a larger difference between the model curves in the higher energy band, future observations in the TeV band will provide results more sensitive to determine the  $E_{\text{max}}$  parameter.

#### 4. Conclusion

We analyzed the GeV gamma-ray emissions in the vicinity of SNR HB9 with the *Fermi*-LAT data spanning for 12 years, aiming to quantify the evolution of DSA. We detected significant gamma-ray emission spatially coinciding with two MCs in the vicinity of the SNR. We found that the gamma-ray spectra above 1 GeV at the cloud regions could be characterized by a simple power-law function with indices of  $1.84 \pm 0.18$  and  $1.84 \pm 0.14$ , which are flatter than that at the SNR shell of  $2.55 \pm 0.10$ . By modeling the diffusion of the CRs that escaped from SNR HB9, we found that the *Fermi*-LAT spectra at the cloud regions could be reproduced with the delayed gamma-ray emission model. Our result implies that the maximum energy with DSA in younger SNRs is likely to be higher than that in older ones. We also found that the Galactic mean value of the diffusion coefficient ( $D_0$ ) is appropriate to explain the observed gamma-ray spectra, indicating that self-confinement by turbulent plasma waves is not effective in the vicinity of SNR HB9. Future

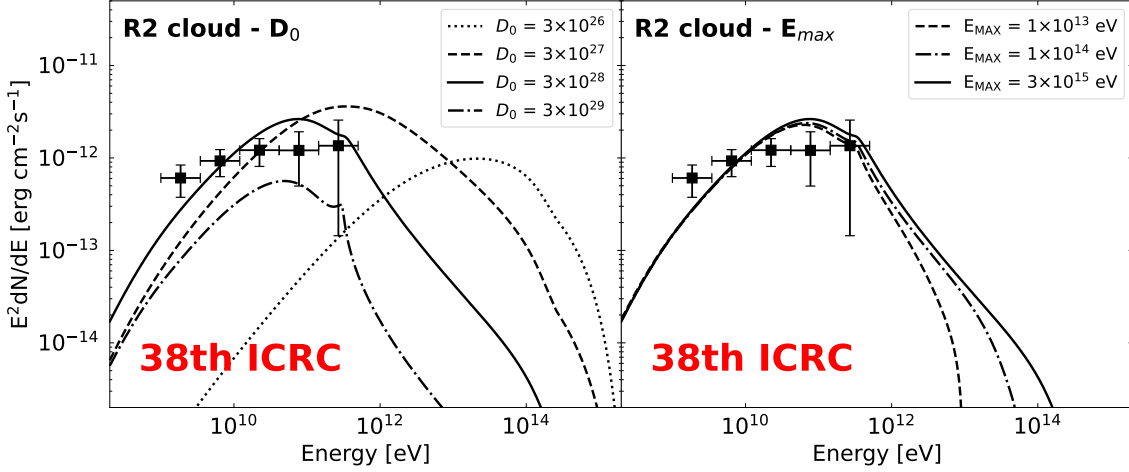


**Figure 4:** Input parameter dependency of the model for the R2 spectrum. **left:** Dependency on  $D_0$  (diffusion coefficient). Dotted, dashed, solid, and dot-dashed curves indicate the models with  $D_0$  of  $3 \times 10^{26} \text{ cm}^2 \text{ s}^{-1}$ ,  $3 \times 10^{27} \text{ cm}^2 \text{ s}^{-1}$ ,  $3 \times 10^{28} \text{ cm}^2 \text{ s}^{-1}$ , and  $3 \times 10^{29} \text{ cm}^2 \text{ s}^{-1}$ , respectively. **right:** Dependency on  $E_{\text{max}}$  (maximum energy of the accelerated particles in the Sedov phase). Dashed, dot-dashed, and solid curves indicate the models with  $E_{\text{max}}$  of  $1 \times 10^{13} \text{ eV}$ ,  $1 \times 10^{14} \text{ eV}$ , and  $3 \times 10^{15} \text{ eV}$ , respectively.

observations in the TeV band will provide results more sensitive to determine the maximum energy of the SNR in the past.

## References

- [1] Oka, T. & Ishizaki, W. 2022, PASJ, 74, 625. doi:10.1093/pasj/psac024
- [2] Baade, W. & Zwicky, F. 1934, Proceedings of the National Academy of Science, 20, 259. doi:10.1073/pnas.20.5.259
- [3] Cristofari, P. 2021, Universe, 7, 324. doi:10.3390/universe7090324
- [4] Ptuskin, V. S. & Zirakashvili, V. N. 2003, A&A, 403, 1. doi:10.1051/0004-6361:20030323
- [5] Gabici, S., Aharonian, F. A., & Blasi, P. 2007, Ap&SS, 309, 365. doi:10.1007/s10509-007-9427-6
- [6] Aharonian, F. A. & Atoyan, A. M. 1996, A&A, 309, 917
- [7] Aharonian, F., Akhperjanian, A. G., Bazer-Bachi, A. R., et al. 2008, A&A, 481, 401. doi:10.1051/0004-6361:20077765
- [8] Uchiyama, Y., Funk, S., Katagiri, H., et al. 2012, ApJL, 749, L35. doi:10.1088/2041-8205/749/2/L35
- [9] Leahy, D. A. & Tian, W. W. 2007, A&A, 461, 1013. doi:10.1051/0004-6361:20065895
- [10] Sezer, A., Ergin, T., Yamazaki, R., et al. 2019, MNRAS, 489, 4300. doi:10.1093/mnras/stz2461

- [11] Araya, M. 2014, MNRAS, 444, 860. doi:10.1093/mnras/stu1484
- [12] Atwood, W. B., Abdo, A. A., Ackermann, M., et al. 2009, ApJ, 697, 1071. doi:10.1088/0004-637X/697/2/1071
- [13] Mattox, J. R., Bertsch, D. L., Chiang, J., et al. 1996, ApJ, 461, 396. doi:10.1086/177068
- [14] Abdollahi, S., Acero, F., Ackermann, M., et al. 2020, ApJS, 247, 33. doi:10.3847/1538-4365/ab6bcb
- [15] Condon, J. J., Broderick, J. J., Seielstad, G. A., et al. 1994, AJ, 107, 1829. doi:10.1086/116992
- [16] Ackermann, M., Ajello, M., Atwood, W. B., et al. 2012, ApJ, 750, 3. doi:10.1088/0004-637X/750/1/3
- [17] Dame, T. M., Hartmann, D., & Thaddeus, P. 2001, ApJ, 547, 792. doi:10.1086/318388
- [18] Taylor, A. R., Gibson, S. J., Peracaula, M., et al. 2003, AJ, 125, 3145. doi:10.1086/375301
- [19] Gabici, S., Aharonian, F. A., & Casanova, S. 2009, MNRAS, 396, 1629. doi:10.1111/j.1365-2966.2009.14832.x
- [20] Ohira, Y., Murase, K., & Yamazaki, R. 2011, MNRAS, 410, 1577. doi:10.1111/j.1365-2966.2010.17539.x
- [21] Ohira, Y., Murase, K., & Yamazaki, R. 2010, A&A, 513, A17. doi:10.1051/0004-6361/200913495
- [22] Zabalza, V. 2015, 34th International Cosmic Ray Conference (ICRC2015), 34, 922
- [23] Dwarakanath, K. S., Shevgaonkar, R. K., & Sastry, C. V. 1982, Journal of Astrophysics and Astronomy, 3, 207. doi:10.1007/BF02714804
- [24] Reich, W., Zhang, X., & Fürst, E. 2003, A&A, 408, 961. doi:10.1051/0004-6361:20030939
- [25] Roger, R. S., Costain, C. H., Landecker, T. L., et al. 1999, A&AS, 137, 7. doi:10.1051/aas:1999239
- [26] Gao, X. Y., Han, J. L., Reich, W., et al. 2011, A&A, 529, A159. doi:10.1051/0004-6361/201016311
- [27] Leahy, D. A. & Aschenbach, B. 1995, A&A, 293, 853
- [28] Dermer, C. D. 1986, A&A, 157, 223
- [29] Fujita, Y., Ohira, Y., Tanaka, S. J., et al. 2009, ApJL, 707, L179. doi:10.1088/0004-637X/707/2/L179
- [30] Yuan, Q., Lin, S.-J., Fang, K., et al. 2017, Phys. Rev. D, 95, 083007. doi:10.1103/PhysRevD.95.083007
- [31] Wentzel, D. G. 1974, ARA&A, 12, 71. doi:10.1146/annurev.aa.12.090174.000443